LETTER • OPEN ACCESS

Multidecadal changes in biology influence the variability of the North Atlantic carbon sink

To cite this article: Clare Ostle *et al* 2022 *Environ. Res. Lett.* **17** 114056

View the article online for updates and enhancements.

ENVIRONMENTAL RESEARCH
LETTERS

LETTER

OPEN ACCESS

Multidecadal changes in biology influence the variability of the North Atlantic carbon sink

Clare Ostle[1,2,*] ⓘ, Peter Landschützer[3,4], Martin Edwards[5,6], Martin Johnson[2,7,8], Sunke Schmidtko[9], Ute Schuster[10], Andrew J Watson[10] and Carol Robinson[2]

1 The Marine Biological Association (MBA), The Laboratory, Citadel Hill, Plymouth PL1 2PB, United Kingdom
2 Centre for Ocean and Atmospheric Sciences (COAS), School of Environmental Sciences, University of East Anglia, Norwich NR4 7TJ, United Kingdom
3 Max Planck Institute for Meteorology, Bundesstr. 53, 20146 Hamburg, Germany
4 Flanders Marine Institute (VLIZ), Jacobsenstraat 1, 8400 Ostend, Belgium
5 Plymouth Marine Laboratory, Prospect Place, Plymouth PL1 3DH, United Kingdom
6 Marine Institute, Plymouth University, Plymouth PL4 8AA, United Kingdom
7 Bantry Marine Research Station, Gearhies, Co. Cork P75 AX07, Ireland
8 Centre for Environment Fisheries and Aquaculture Science (Cefas), Lowestoft NR33 0HT, United Kingdom
9 GEOMAR Helmholtz Centre for Ocean Research Kiel, 24105 Kiel, Germany
10 College of Life and Environmental Sciences, University of Exeter, Exeter EX4 4QE, United Kingdom
* Author to whom any correspondence should be addressed.

E-mail: claost@mba.ac.uk

Abstract

The North Atlantic Ocean is the most intense marine sink for anthropogenic carbon dioxide (CO_2) in the world's oceans, showing high variability and substantial changes over recent decades. However, the contribution of biology to the variability and trend of this sink is poorly understood. Here we use *in situ* plankton measurements, alongside observation-based sea surface CO_2 data from 1982 to 2020, to investigate the biological influence on the CO_2 sink. Our results demonstrate that long term variability in the CO_2 sink in the North Atlantic is associated with changes in phytoplankton abundance and community structure. These data show that within the subpolar regions of the North Atlantic, phytoplankton biomass is increasing, while a decrease is observed in the subtropics, which supports model predictions of climate-driven changes in productivity. These biomass trends are synchronous with increasing temperature, changes in mixing and an increasing uptake of atmospheric CO_2 in the subpolar North Atlantic. Our results highlight that phytoplankton play a significant role in the variability as well as the trends of the CO_2 uptake from the atmosphere over recent decades.

1. Introduction

Marine phytoplankton are responsible for approximately half of the primary production on earth [1]. However, little is known about how variable the biological response to interannual changes in ocean circulation is, and how this is influencing the air-sea flux of carbon dioxide (CO_2). This is in part due to a lack of *in situ* measurements [2, 3], which has led to a substantial divergence in future climate model projections [4, 5]. Therefore, quantifying the role of phytoplankton in marine carbon sequestration is critical in understanding the biological impacts of climate change and consequent feedbacks on climate.

Atmospheric CO_2 concentrations have increased continuously since the industrial revolution, contributing to rising global temperatures [6]. The North Atlantic Ocean is an important net sink of atmospheric CO_2, taking up an estimated 23% of the anthropogenic global carbon inventory, while only covering 15% of the global ocean [7, 8]. CO_2 uptake in the North Atlantic is highly variable [9, 10], with air-sea exchange controlled by the partial pressure CO_2 (pCO_2) gradient between the ocean and the

atmosphere, which is influenced by the temperature dependent solubility of CO_2 as well as other processes such as physical mixing and biological uptake [10, 11]. While the influence of temperature on the solubility of pCO_2 is well understood [11–13], much less process understanding exists regarding the drivers that are not directly related to temperature variations, i.e. the non-thermal drivers, in particular the role of biology. Ocean circulation and mixing control the amount of deep, aged (i.e. carbon and nutrient rich) water reaching the ocean surface [14–16], and therefore modify on large scales, the magnitude of biological production. Seasonal warming and light, as well as nutrient availability, trigger phytoplankton photosynthesis, with consequent increased uptake of CO_2 [12] and increase in phytoplankton biomass. Satellite measurements have served as appropriate indicators of the variability in sea-surface chlorophyll-*a* (chl-*a*), i.e. a first order proxy for biological production in the top surface layer of the ocean, but are not yet able to differentiate the plankton community composition [17–19]. Here we also use *in situ* data collected from the Continuous Plankton Recorder (CPR), which utilises a robust marine sampler towed within surface waters at a depth of ∼7 m (sampling the top ∼20 m of seawater due to the wash of the volunteer ships that tow CPRs) and a procedure that has remained consistent since 1958 [20]. This unique dataset allows us to investigate the variability of plankton biomass and community composition in surface waters over multiple decades at large spatial scales, such as that of the North Atlantic Ocean. Combining this with an observation-based estimate of the partial pressure of carbon dioxide (pCO_2) at the sea surface [21, 22] from 1982 to 2020 derived from the Surface Ocean CO_2 Atlas (SOCAT) [23], we demonstrate the importance of biology on the uptake of carbon in the North Atlantic at seasonal, interannual and decadal time-scales. Further, by investigating changes in temperature and mixing, we provide a more advanced understanding of the processes involved in the drawdown of CO_2.

2. Materials and methods

Our main focus here is the basin-wide relationship between phytoplankton and the difference in atmospheric and oceanic CO_2 concentrations, i.e. the thermodynamic disequilibrium driving the exchange of CO_2 between the atmosphere and the surface ocean of the North Atlantic (See figure S1 for mean values and study area). The air-sea pCO_2 difference ($pCO_2^{sea} - pCO_2^{atm} = \Delta pCO_2$), was calculated using xCO_2 atmospheric data obtained from the NOAA marine boundary layer reference network [24]. Phytoplankton groups were defined and quantified using CPR data [20], and diatoms are presented in the main text, however other phytoplankton groupings were considered in the analysis (table S1

within the supplementary extended data lists the phytoplankton taxa that were included in the phytoplankton groupings for diatoms and dinoflagellates. Coccolithophores and silicoflagellates were included as separate groups and were only recorded as presence/absence values until 1993, after which they are routinely speciated and counted within the CPR survey, however their pigment (along with other phytoplankton species' pigment) is detected in the Phytoplankton Colour Index (PCI) signal [20]. Diatoms are also thought to be one of the major phytoplankton groups contributing to the biological uptake and potential export of CO_2, due to their relative size (and therefore transfer efficiency to the deep ocean) and dominance of the North Atlantic spring bloom [25, 26].

2.1. Datasets

The carbon observation data were obtained from the SOCAT (www.socat.info) [23]. pCO_2 is derived from the fugacity of carbon dioxide (fCO_2) [27] and then interpolated using a 2-step neural network technique to provide monthly coverage on a $1 \times 1°$ grid [21, 22].

Regional monthly-mean atmospheric xCO_2 data were obtained from the NOAA marine boundary layer reference network [24]. This was converted to atmospheric pCO_2 following [28]:

$$pCO_2^{atm} = xCO_2^{atm} \times (P - P_{H_2O}) \qquad (1)$$

where P is the sea-level pressure [29], and P_{H_2O} is the water-vapour pressure at 100% humidity [28].

The phytoplankton data were obtained from the CPR Survey (CPR, www.cprsurvey.org). The CPR is a towed marine sampler, that is voluntarily towed behind ships of opportunity at a water depth of ∼7 m, which due to the wash of the ship samples the top ∼20 m surface layer [20]. The mesh size of the silk used within the CPR is 270 μm, and although this means that larger phytoplankton are better represented in the CPR dataset, the CPR does routinely record phytoplankton down to approx. 5–10 μm (such as coccolithophores). In addition, the PCI does reflect some of the smaller taxa as their biomass adds to the colouration of the silk [30]. Satellite derived chl-*a* was also included in the analysis as an independent measure of phytoplankton biomass within the study area. It is important to note that there are limitations associated with both satellite and CPR measurements for estimating the plankton [18], as with any plankton sampling method [31]. Rare species bias was removed from the CPR dataset by only including taxa that occur above 1% frequency of occurrence [32]. Table S1 within the supplementary extended data lists the taxa that were included in the phytoplankton groups, as well as the use of the PCI. The phytoplankton data were all log transformed using $\log_{10}(x+1)$ in order to homogenise the variance [33, 34]. Each phytoplankton index was gridded onto a $1 \times 1°$ grid by taking the monthly mean for each grid cell, and removing

any grid cell where the CPR sample number was <3 to reduce the potential impact of decreased sampling effort [34]. For a detailed methodology on using the CPR data please refer to Richardson *et al* [20].

The satellite derived estimate of sea surface chl-*a* was obtained from the OC-CCI dataset version 4.1, which is a merged MERIS, Aqua-MODIS, SeaWiFS and VIIRS global satellite product from 1998–present (esa-oceancolour-cci.org) [35]. The chl-*a* data were averaged by month on to a $1 \times 1°$ grid within the study area for the analysis.

Mean monthly sea surface temperature (SST) data from 1982 to 2020 were obtained from the International Comprehensive Ocean-Atmosphere Data Set (ICOADS, 1° enhanced data, www.esrl.noaa.gov/psd/data/gridded/data.coads.1deg.html) [36].

Mixed layer depth (MLD) from 1982 to 2020 was obtained from the global ocean and sea-ice reanalysis products (ORAS5: Ocean Reanalysis System 5) prepared by the European Centre for Medium-Range Weather Forecasts (ECMWF www.ecmwf.int/node/18519) [37] and generated using Copernicus Climate Change Service information (2022). Where MLD is defined as the depth of the ocean where the average sea water density exceeds the near surface density plus 0.01 kg m^{-3}.

2.2. Data collocation
Datasets were spatio-temporally collocated by gridding them at $1 \times 1°$ resolution and taking monthly means within each grid cell from 1982 to 2020, with the exceptions of the chl-*a* dataset which was only available from 1998 onwards. Although CPR data from the North Atlantic are available from 1958 onwards, for comparison with oceanic CO_2 data (available from 1982 onwards) the main analyses within this paper focus on the period 1982 to 2020, however phytoplankton trends are presented in figure 6 to aid discussion around multidecadal trends.

2.3. Thermal and non-thermal pCO_2 components
Thermal (pCO_2T) and non-thermal (pCO_2NT) driving components on pCO_2 were derived based on the well constrained influence of temperature on pCO_2 under fixed dissolved inorganic carbon (DIC) and total alkalinity (TA) conditions, where $\partial \ln pCO_2 / \partial T = 0.04231 °C^{-1}$ [11–13]:

$$pCO_2T = \overline{pCO_2} \times e^{0.04231 \times (SST - \overline{SST})} \qquad (2)$$

$$pCO_2NT = pCO_2 \times e^{0.04231 \times (\overline{SST} - SST)} \qquad (3)$$

where the over bar indicates mean parameter. pCO_2T calculated following equation (2) represents the pCO_2 concentration if the addition or removal of carbon by biological and air-sea exchange processes were absent. pCO_2NT (equation (3)) represents the pCO_2 concentration due to changes in DIC and TA, which could be influenced by biology, air-sea CO_2 exchange, advection, and mixing [13].

2.4. Determination of linear trends and statistical testing
Annual linear trends were calculated for each $1 \times 1°$ grid-cell, using standard model I linear regression. The significance of the linear trend was calculated whereby the ratio (*tb*) of the linear trend (*T*) and the standard error of the linear trend (*SE(Ne)*) (equation (5)) were compared to a critical value of *t* (*tcrit*, assuming a distribution of student's t) at a 95% significance level and the effective degrees of freedom, which takes into account any autocorrelation within the time-series by using the effective sample size (*Ne*) [38]:

$$tb > tcrit(0.95, Ne - 2) = \text{significant} \qquad (4)$$
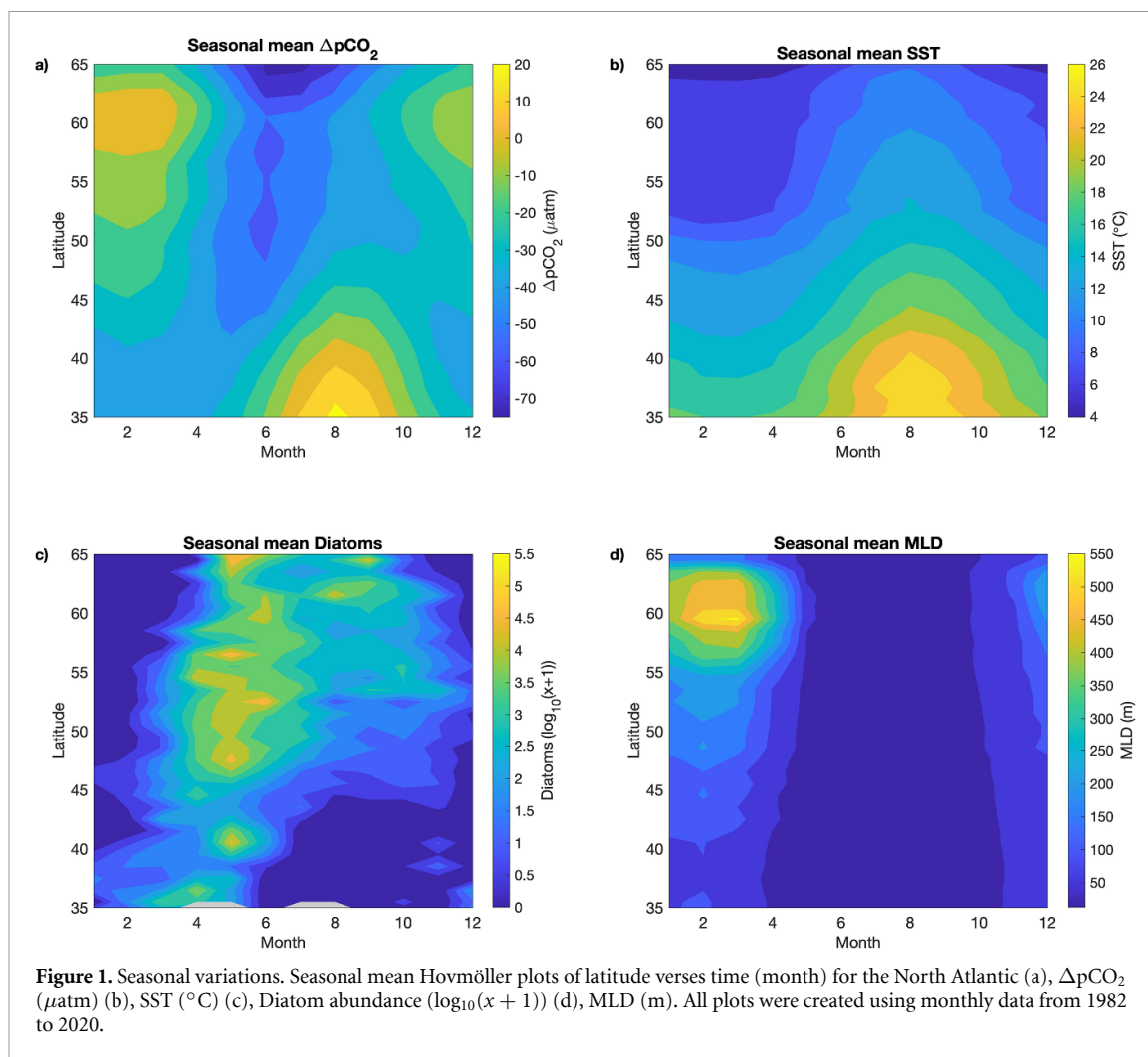
$$tb = \frac{T}{SE(Ne)}. \qquad (5)$$

The most common autocorrelation within time-series is temporal autocorrelation, which implies that throughout time preceding observations are not independent of each other. This has implications for the significance of any trend where temporal autocorrelation exists [39]. To account for temporal autocorrelation when calculating the significance of the linear trends and any correlations within the time-series data, the modified Chelton method was used as it has been shown to be the optimum method for altering significance due to autocorrelation within time-series [39]. Those samples that are not autocorrelated within the time-series are effectively independent and counted within the effective sample size (*Ne*), which will be less than the sample size (*N*). By using the effective sample size to calculate the standard error of the linear trend and the critical value of *t* (rather than *N*) this reduces the significance of the trends and therefore takes into account autocorrelation within the time-series [40].

2.5. Objective mapping
Objective mapping was used for gap-filling of the CPR values in figures 4(c) and S1(c), for all other visualisations or numerical results no gap-filling technique was used on the CPR data. Objective mapping is similar to kriging and follows the least squares approach, but it assumes that the mean drift (trend) is known and uses a covariance matrix where larger weights are assigned to points that are nearby and co-vary positively with the estimated values [41]. The method can be described by the following equation:

$$b = w \times E^{-1} \times r \qquad (6)$$

where *b* is the mapped property, *w* is the data weights, *E* is the covariance matrix and *r* is the residuals (weighted mean) [42].

Figure 1. Seasonal variations. Seasonal mean Hovmöller plots of latitude verses time (month) for the North Atlantic (a), $\Delta p CO_2$ (μatm) (b), SST (°C) (c), Diatom abundance ($\log_{10}(x+1)$) (d), MLD (m). All plots were created using monthly data from 1982 to 2020.
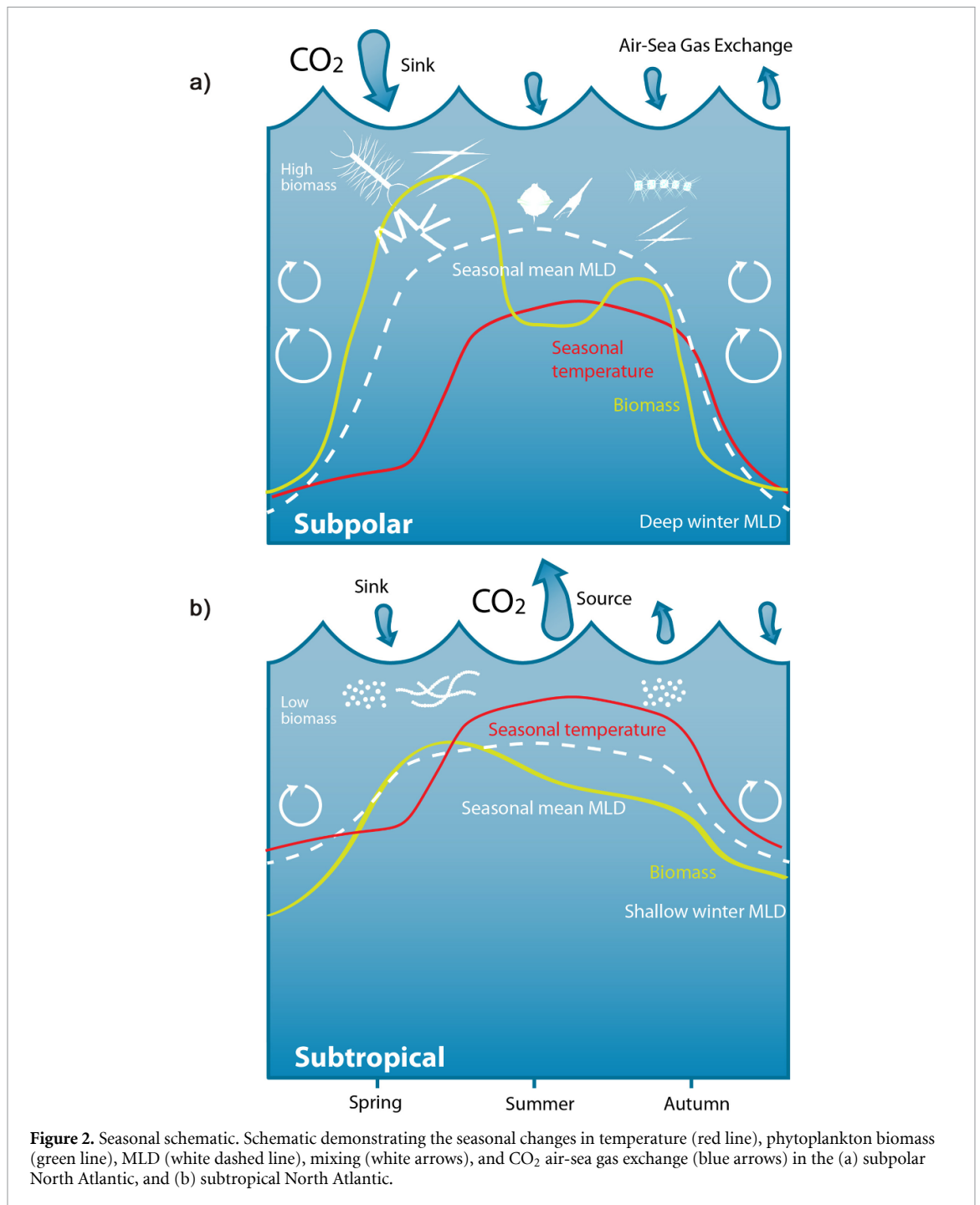
2.6. Monthly standardised anomalies

Standardised zscore calculation measures the standardisation (distance from the mean using standard deviation) of the data [41]. The output is a standardized zscore where positive values signify values above the long term mean and negative values are below the long term mean, zero values are at the long term mean.

3. Results and discussion

Our analysis reveals that the seasonal diatom abundance maxima occurred concurrently with the seasonal minima in $\Delta p CO_2$ (figures 1(a) and (c)). In temperate and subpolar latitudes this occurs during spring. Further south, in the subtropical zone, where temperature dominates the timing of the seasonal carbon maximum [11, 12, 43], diatoms and $\Delta p CO_2$ have their seasonal maximum/minimum shifted towards winter. This confirms that two contrasting mechanisms are affecting the seasonal cycle of CO_2 drawdown in the North Atlantic [21, 43]. In higher latitudes, the strongest drawdown of sea surface CO_2 is observed during spring (figure 1(a)), initiated by a combination of increasing light levels, rising temperatures
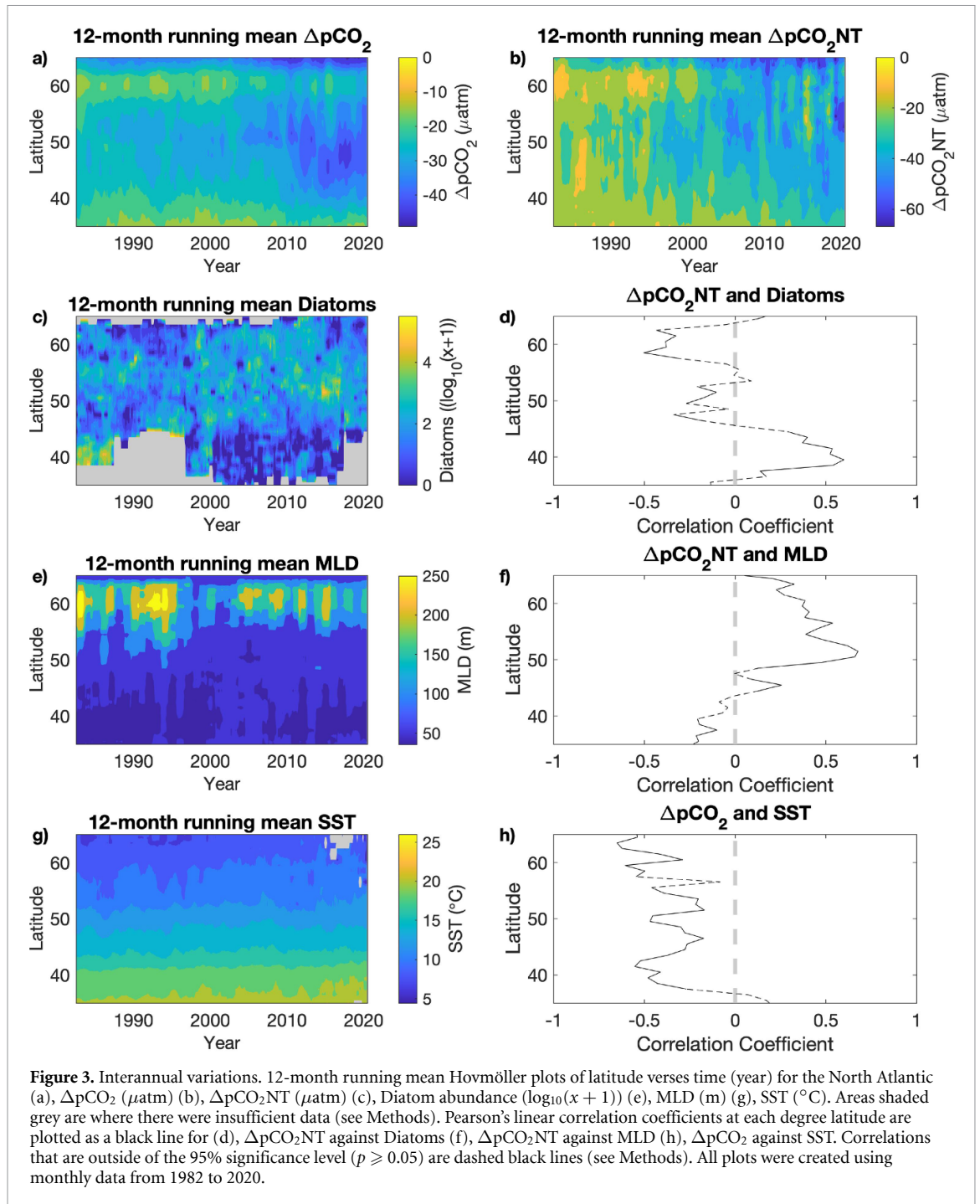
(figure 1(b)), and by increased nutrient concentrations brought to the surface by deep wintertime mixing (figure 1(d)). This spring period is associated with a peak in spring-blooming diatoms during May/June (figure 1(c)). At these higher latitudes, there is also a later, weaker CO_2 drawdown period in August associated with diatom biomass (figures 1(a) and (c)). In the high latitudes in winter, the seasonal $\Delta p CO_2$ signal (figure 1(a)) is positive, i.e. the surface ocean is supersaturated with CO_2 with respect to the atmospheric concentration. This supersaturation is associated with increased turbulence (MLD) (figure 1(d)) that is mixing carbon-rich deeper waters to the surface [13]. As temperatures increase and surface wind speeds decrease in spring, stratification allows the phytoplankton to bloom and take up CO_2 via photosynthesis, making the surface ocean CO_2 undersaturated with respect to the atmospheric CO_2 [13] (negative $\Delta p CO_2$). The seasonal temperature cycle is opposing the sea-surface $\Delta p CO_2$ in the high latitudes (figures 1(a) and (b)), confirming that solubility only plays a secondary role in the $\Delta p CO_2$ seasonality [11, 21, 43]. In contrast, in the lower latitudes, the solubility effect is the dominant process [11], as the seasonal $\Delta p CO_2$ cycle follows the seasonal

Figure 2. Seasonal schematic. Schematic demonstrating the seasonal changes in temperature (red line), phytoplankton biomass (green line), MLD (white dashed line), mixing (white arrows), and CO_2 air-sea gas exchange (blue arrows) in the (a) subpolar North Atlantic, and (b) subtropical North Atlantic.

temperature variability with summer/autumn months being associated with the release of CO_2 to the atmosphere from the ocean (figures 1(a) and (b)) [21, 43]. These contrasting mechanisms between the subpolar and subtropical North Atlantic are schematically illustrated in figure 2.

On interannual time-scales, the comparison between the $\Delta p CO_2$ and its drivers (figure 3) illustrates that year-to-year changes in the North Atlantic carbon sink are largely driven by non-thermal effects. Here we derive the temperature independent $\Delta p CO_2$ (non-thermal $\Delta p CO_2$NT, see figure 3(b)) using the temperature sensitivity of CO_2 in seawater [11–13] (see Methods). The $\Delta p CO_2$NT represents changes

in $p CO_2$ due to non-thermal drivers such as; ocean circulation, mixing, air-sea exchange and biological processes [13]. As the temporal variability of ocean $p CO_2$ is larger than that of atmospheric $p CO_2$ [24, 44, 45], the interannual variability in the $\Delta p CO_2$ is likely to be a product of changes in temperature, ocean physics and biology (figures 3(c), (e) and (g)), and not atmospheric variability. From 2010 onwards, we find a substantial decrease in the seawater $\Delta p CO_2$ and $\Delta p CO_2$NT at ~50° N (figures 3(a) and (b)). This more negative $\Delta p CO_2$ indicates an increased uptake of CO_2 by the ocean, which corresponds to an increasing trend in SST, shoaling of the mixed layer and an increase in diatom abundance

Figure 3. Interannual variations. 12-month running mean Hovmöller plots of latitude verses time (year) for the North Atlantic (a), $\Delta p CO_2$ (μatm) (b), $\Delta p CO_2 NT$ (μatm) (c), Diatom abundance ($\log_{10}(x+1)$) (e), MLD (m) (g), SST (°C). Areas shaded grey are where there were insufficient data (see Methods). Pearson's linear correlation coefficients at each degree latitude are plotted as a black line for (d), $\Delta p CO_2 NT$ against Diatoms (f), $\Delta p CO_2 NT$ against MLD (h), $\Delta p CO_2$ against SST. Correlations that are outside of the 95% significance level ($p \geqslant 0.05$) are dashed black lines (see Methods). All plots were created using monthly data from 1982 to 2020.

(figures 3(c), (e) and (g)). We interpret this signal as indicative of shallower mixing depths reducing light limitation, therefore leading to increased photosynthesis, and hence increased uptake of CO_2 from the water. The observed increased phytoplankton biomass (figure 6(a)) is dominated by an increase in diatoms (figure 3(c)) and coccolithopheres (figure 6(e)) during this period. The $\Delta p CO_2$ variation and smaller difference between the air-sea $p CO_2$ during the 1990s at 60° N (figures 3(a) and (b), ~60° N) aligns with the increased mixing that occurred during this period as the Labrador Sea convection increased [46, 47], bringing carbon-rich waters to the surface and lower diatom abundance due to stronger

vertical mixing and hence limited light availability (figures 3(c), (e) and 4(a), (e)). Correlation between diatom abundance and $\Delta p CO_2 NT$ are negative in the subpolar ($\geqslant 45.5°$ N) and positive in the subtropical ($< 45.5°$ N) North Atlantic, whilst throughout the majority of the North Atlantic, SST shows a negative correlation with $\Delta p CO_2$ (figure 3(h)), and MLD shows the expected positive correlation with $\Delta p CO_2 NT$ (figure 3(f)). This confirms the strong link between CO_2, phytoplankton biomass and mixing, because if it were just temperature driving the interannual variability you would expect to see a significant positive correlation between $\Delta p CO_2$ and SST across all latitudes.

Figure 4. Linear trends. Linear trend maps for; (a), ΔpCO_2 (μatm yr^{-1}), (c), Diatom abundance ($\log_{10}(x+1)$ yr^{-1}), (e), MLD (m yr^{-1}), (g), SST (°C yr^{-1}), (i), chl-*a* (miiligram m^{-3} yr^{-1}). Red shades signify an increasing trend while blue shades signify a decreasing trend from 1982–2020, except for chl-*a* (1998–2020). Areas shaded grey are where there were insufficient data (see Methods).
Note: Objective mapping was used to interpolate the diatom data for mapping (see Methods). Respective standardised monthly anomalies (see Methods) within the subpolar North Atlantic (blue, $\geqslant$45.5° N) and the subtropical North Atlantic (red, <45.5° N) for (b), ΔpCO_2 (μatm), (d), Diatoms ($\log_{10}(x+1)$), (f), MLD (m), (h), SST (°C, (j), chl-*a* (miiligram m^{-3}), with the linear trend line and significance shown.

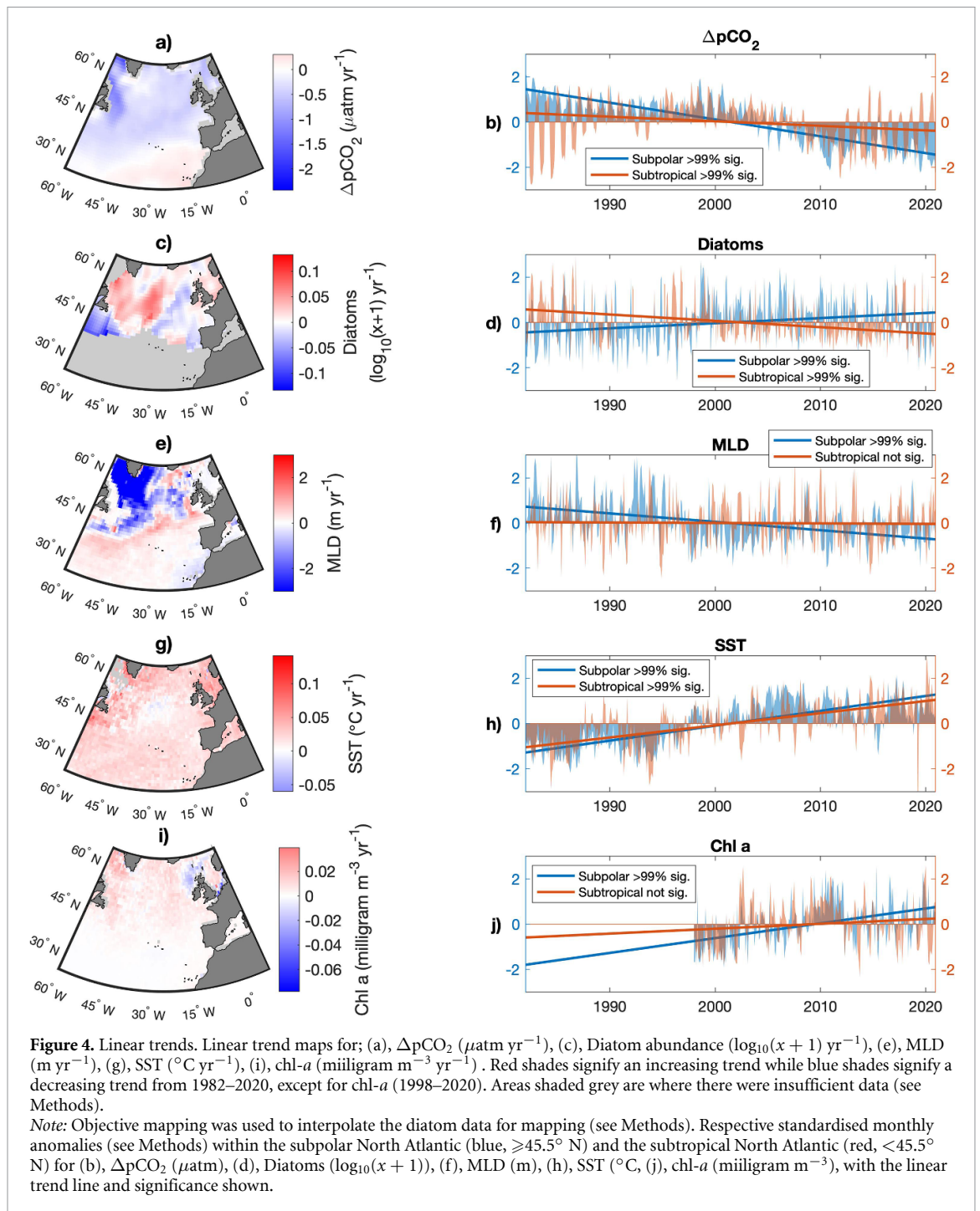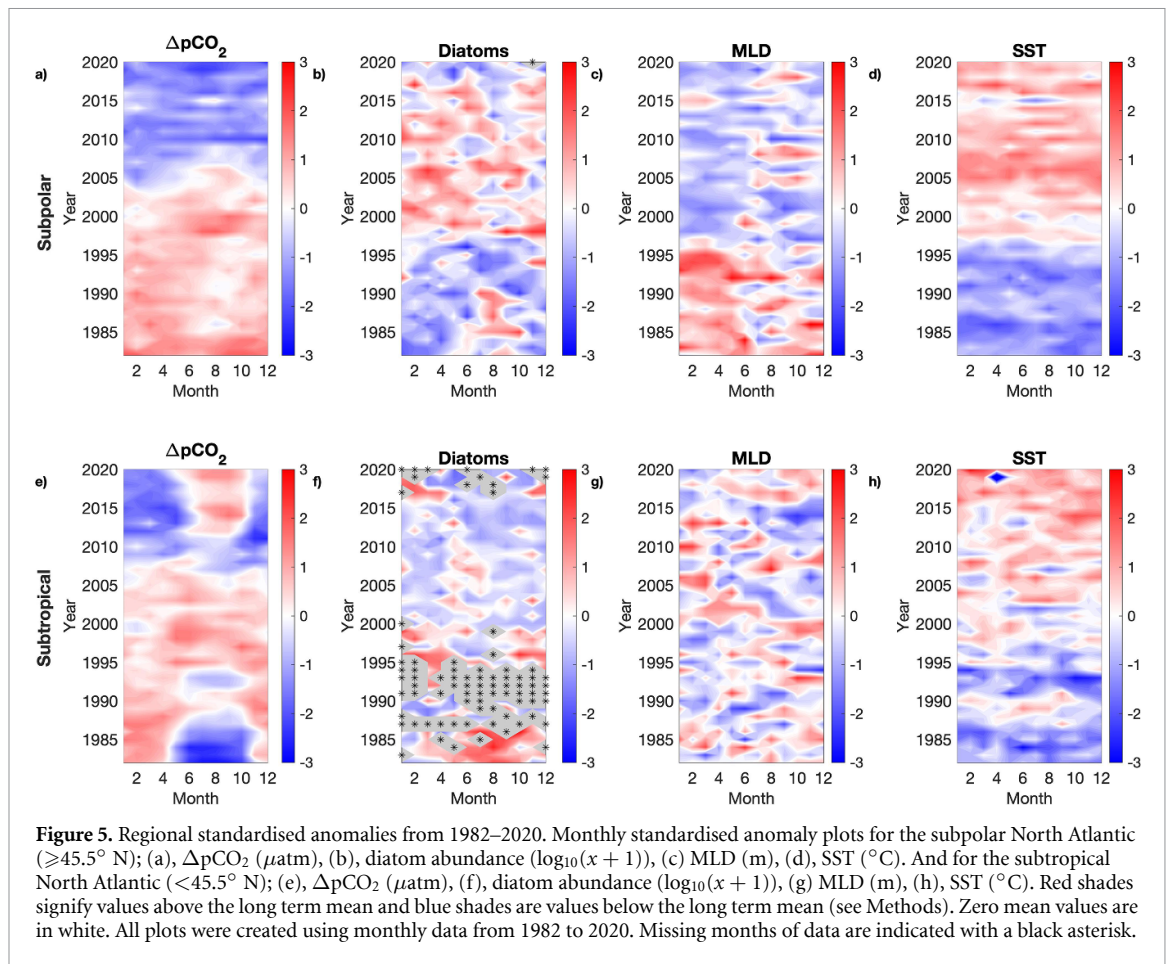Figure 4 shows maps of the annual linear trends in ΔpCO_2, CPR diatom abundance, MLD, SST and satellite derived chl-*a* estimates for the study area, alongside time-series of the standardised monthly anomalies and linear trends within the the subpolar North Atlantic ($\geqslant$45.5° N) and the subtropical North Atlantic (<45.5° N) (see Methods). Across most of the North Atlantic the ΔpCO_2 sink is increasing (decreasing trend = more uptake to the ocean), with a significant decrease in ΔpCO_2 seen within the subpolar and subtropical North Atlantic (figures 4(a) and (b)). Although diatom abundance has increased across most of the study area, there is a pattern of

decreasing abundance towards the subtropical North Atlantic (figures 4(c) and (d)). This regional biomass trend is also reflected in the PCI (PCI, figure 6), and although the satellite derived chl-*a* data only started in 1998, an increase in chl-*a* is also observed across most of the subpolar region (figures 4(i) and (j)). SST has increased across the study area (figures 4(g) and (h)), whereas MLD shows a decrease across most of the subpolar North Atlantic, in particular the western North Atlantic (figure 4(e)). This pronounced shoaling of the mixed layer in the Labrador Sea since the end of the 1990s (figures 4(e) and (f)), coincides with increased diatom abundance which is more

Figure 5. Regional standardised anomalies from 1982–2020. Monthly standardised anomaly plots for the subpolar North Atlantic ($\geqslant$45.5° N); (a), ΔpCO_2 (μatm), (b), diatom abundance ($\log_{10}(x+1)$), (c) MLD (m), (d), SST (°C). And for the subtropical North Atlantic (<45.5° N); (e), ΔpCO_2 (μatm), (f), diatom abundance ($\log_{10}(x+1)$), (g) MLD (m), (h), SST (°C). Red shades signify values above the long term mean and blue shades are values below the long term mean (see Methods). Zero mean values are in white. All plots were created using monthly data from 1982 to 2020. Missing months of data are indicated with a black asterisk.

pronounced on the western North Atlantic because of a reduction in Labrador Sea convection due to warming [46, 47] (figures 4(c) and (d)). These data support model predictions suggesting that increasing temperature would result in enhanced stratification which would lead to decreased productivity in the subtropics due to increased nutrient limitation and increased productivity in subpolar regions due to decreased light limitation [48–51]. Figures 5 and 6 (phytoplankton groups) depict these regional changes between the subpolar and subtropical North Atlantic, showing how mean seasonality and annual variability change over time (see Methods). Despite no clear correspondence between interannual variability in SST and CO_2 (figure 3), we do find a corresponding long term warming trend in the subpolar region that matches a long term increase in the CO_2 sink which likely reflects the continued increase in atmospheric pCO_2 concentrations [5] (figures 5(a) and (d)). We find a significant decrease in ΔpCO_2 in the higher latitudes of -0.45 ± 0.03 μatm yr^{-1} implying an increase in the marine carbon sink (figures 4(a), (b) and 5(a)), see supplementary extended data table S2 for trend values and their uncertainties). This sink is associated with increased productivity in the subpolar North Atlantic, increased mixing within the Labrador Sea and decreased mixing within

the central subpolar North Atlantic (figures 4(a), (c), (e) and 5, supplementary figure 6 and table S2). In the region defined here as subtropical(<45.5° N), it appears that there has been a shift from a seasonal ocean decrease in CO_2 during the summer months when Diatom abundance was high (1980s), to a seasonal increase in CO_2 during the summer months (2010–2020) where increased temperatures and low Diatom abundance appear to be dominating the system (figures 5(e)–(h)). Over decadal time periods, regional natural variability is likely to be affecting the processes that influence carbon flux variability with varying influence in different regions of the North Atlantic [22, 52]. In particular, the North Atlantic Oscillation has been shown to influence the circulation between the subtropical and subpolar gyres at the decadal scale [8, 52].

The PCI presents a significant increasing trend across the whole North Atlantic since 1958 (see figure 6). This suggests that smaller phytoplankton taxa (<5 μm) might be increasing across the whole North Atlantic as they are represented in the PCI but not always recorded in the taxonomic identification process due to the semi-quantitative nature of the CPR sampling (see Methods) and the difficulty of identifying smaller phytoplankton using light microscopy. This observation is supported by both the
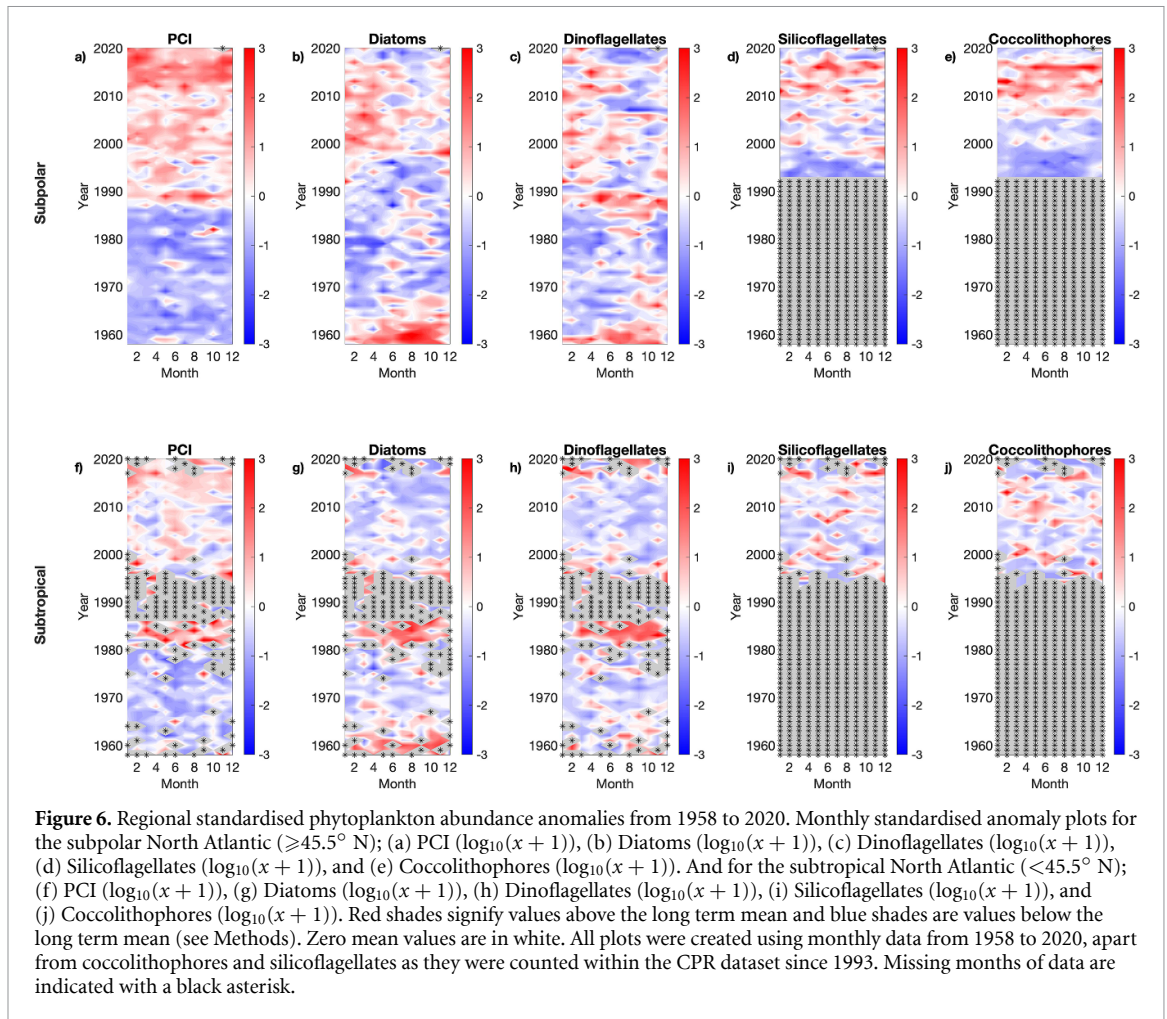
Figure 6. Regional standardised phytoplankton abundance anomalies from 1958 to 2020. Monthly standardised anomaly plots for the subpolar North Atlantic ($\geqslant$45.5° N); (a) PCI ($\log_{10}(x + 1)$), (b) Diatoms ($\log_{10}(x + 1)$), (c) Dinoflagellates ($\log_{10}(x + 1)$), (d) Silicoflagellates ($\log_{10}(x + 1)$), and (e) Coccolithophores ($\log_{10}(x + 1)$). And for the subtropical North Atlantic (<45.5° N); (f) PCI ($\log_{10}(x + 1)$), (g) Diatoms ($\log_{10}(x + 1)$), (h) Dinoflagellates ($\log_{10}(x + 1)$), (i) Silicoflagellates ($\log_{10}(x + 1)$), and (j) Coccolithophores ($\log_{10}(x + 1)$). Red shades signify values above the long term mean and blue shades are values below the long term mean (see Methods). Zero mean values are in white. All plots were created using monthly data from 1958 to 2020, apart from coccolithophores and silicoflagellates as they were counted within the CPR dataset since 1993. Missing months of data are indicated with a black asterisk.

silicoflagellate and coccolithophore phytoplankton groupings (which generally include smaller taxa than the diatom and dinoflagellate taxa presented (table S1)) showing significant increases in the subpolar region, however their abundance has only been counted since 1993 (figure 6). Changes in dinoflagellate abundance show a similar pattern to that of the diatoms (figure 6), however this could be due to the CPR not quantitatively sampling some of the smaller less-robust dinoflagellate taxa. If modelled predictions of declines in productivity and plankton cell-size are correct [48–51], then it is likely that carbon export and potential sequestration to the deep ocean will be reduced, due to a decreased transfer efficiency [4]. Climatic indices will also likely be influencing multidecadal changes in the phytoplankton [53]. Edwards *et al* [54] demonstrated that the Atlantic Multidecadal Oscillation (AMO) coupled with the Northern Hemisphere Temperature anomaly is a strong driver of diatom abundance in the northeast Atlantic. These results support our findings, as we see a shift during the 1990s in all of our phytoplankton groupings (see figure 6) which coincides with when the AMO shifts from a negative phase to a positive phase alongside increasing temperatures. This

natural climate variability, coupled with warming due to climate change is therefore likely adding to the strength of the trends reported here and demonstrates the regional complexity needed for global models.

4. Conclusion

Our results indicate that marine primary production does not simply affect the (sub-) annual ocean uptake of CO_2 from the atmosphere, but it also significantly correlates with the long term variability of this uptake. Our observation-based study agrees with past productivity modelling studies, which have suggested opposing trends in productivity between the subpolar and subtropical North Atlantic [48–51]. However, if the current temperature trajectory and changes in mixing conditions continues, then global declines of productivity could occur, as the balance between relief of light limitation and strengthening nutrient limitation caused by stronger and longer stratification, is altered [51, 55]. The varying influence (from seasonal to multidecadal) of biology on the variability of carbon uptake should be included in models aiming to predict future carbon uptake scenarios. The current ability to represent biological

processes in global marine models is limited [56], yet essential for capturing the variability of our climate at multidecadal scales. Although our correlation analysis does not permit us to further untangle the non-thermal drivers and quantify the relative contributions of biology and physics separately, it is encouraging that these data, derived from independent sources and *in situ* observations, complement each other so clearly, and are consistent with our understanding and model predictions of the system. Our results highlight that phytoplankton play a fundamental role in ocean carbon uptake and its long term variability, therefore regulating the earth's climate. The role of phytoplankton role in this process is dictated by the community composition (predominantly diatoms in the North Atlantic), the latitude (subpolar systems drawing down more carbon) and by large-scale hydro-climatic processes operating over multidecadal scales. Only by the sustained and coordinated monitoring of these oceanic biogeochemical parameters and plankton communities can we improve our understanding of future climate change impacts and the role of the ocean in planetary feedback mechanisms, which are currently poorly constrained in areas with complex bio-physical interactions of carbon uptake.

Data availability statement

The data that support the findings of this study are available upon reasonable request from the authors. The datasets that support the findings of this study are available through the following listed websites; the carbon observation data were obtained from the SOCAT (www.socat.info), the biological data were obtained from the CPR Survey (www.cprsurvey.org), SST data were obtained from the ICOADS (1° enhanced data, www.esrl.noaa.gov/psd/data/gridded/data.coads.1deg.html). The satellite derived estimate of sea surface chl-*a* was obtained from the OC-CCI dataset version 4.1 (esa-oceancolour-cci.org) [35]. MLD was obtained from the global ocean and sea-ice reanalysis products (ORAS5: Ocean Reanalysis System 5) prepared by the European Centre for Medium-Range Weather Forecasts (ECMWF www.ecmwf.int/node/18519) [37].

Author contributions

C R, U S, M E conceived the project, P L developed the neural network analysis, C O collated the data, did the computations and data analysis and prepared the first draft of the manuscript. A J W provided expertise on ocean circulation and biogeochemical processes, M J, S S and P L provided expertise on computations. M E developed the illustrative schematic. All authors contributed to the discussion of the results and reviewed the manuscript.

Conflict of interest

The authors declare that they have no conflicts of interests.

ORCID iD

Clare Ostle ⬤ https://orcid.org/0000-0001-6923-5535

References

[1] Falkowski P 2012 Ocean science: the power of plankton *Nature* **483** S17–S20

[2] Bennington V, McKinley G A, Dutkiewicz S and Ullman D 2009 What does chlorophyll variability tell us about export and air-sea CO_2 flux variability in the North Atlantic? *Glob. Biogeochem. Cycles* **23** 1–11

[3] Fay A R and McKinley G A 2017 Correlations of surface ocean pCO_2 to satellite chlorophyll on monthly to interannual timescales *Glob. Biogeochem. Cycles* **31** 436–55

[4] Henson S A Laufkötter C, Leung S, Giering S L C, Palevsky H I and Cavan E L 2022 Uncertain response of ocean biological carbon export in a changing world *Nat. Geosci.* **15** 248–54

[5] Friedlingstein P *et al* 2022 Global carbon budget 2021 *Earth Syst. Sci. Data* **14** 1917–2005

[6] Hartmann D L *et al* 2013 Observations: atmosphere and surface *Climate Change 2013: The Physical Science Basis: Contribution of Working Group I to the Fifth Assessment Report of the Intergovernmental Panel on Climate Change* (Cambridge: Cambridge University Press)

[7] Sabine C L *et al* 2004 The oceanic sink for anthropogenic CO_2 *Science* **305** 367–71

[8] Schuster U, Watson A and Bates N 2009 Trends in North Atlantic sea-surface fCO2 from 1990 to 2006 *Deep Sea Res.* II **56** 620–9

[9] Watson A J *et al* 2009 Tracking the variable North Atlantic sink for atmospheric CO_2 *Science* **326** 1391–3

[10] McKinley G a, Fay A R, Takahashi T and Metzl N 2011 Convergence of atmospheric and North Atlantic carbon dioxide trends on multidecadal timescales *Nat. Geosci.* **4** 606–10

[11] Takahashi T and Sutherland S 2002 Global sea-air CO_2 flux based on climatological surface ocean p CO_2 and seasonal biological and temperature effects *Deep Sea Res.* II **49** 1601–22

[12] Takahashi T, Olafsson J, Goddard J G, Chipman D W and Sutherland S C 1993 Seasonal variation of CO_2 and nutrients in the high-latitude surface oceans: a comparative study *Glob. Biogeochem. Cycles* **7** 843–78

[13] Körtzinger A *et al* 2008 The seasonal pCO_2 cycle at 49N/16.5W in the northeastern Atlantic Ocean and what it tells us about biological productivity *J. Geophys. Res.* **113** C04020

[14] Landschützer P *et al* 2015 The reinvigoration of the Southern Ocean carbon sink *Science* **349** 1221–4

[15] Devries T, Holzer M and Primeau F 2017 Recent increase in oceanic carbon uptake driven by weaker upper-ocean overturning *Nature* **542** 215–18

[16] DeVries T *et al* 2019 Decadal trends in the ocean carbon sink *Proc. Natl Acad. Sci.* **116** 201900371

[17] Behrenfeld M J O'Malley R T, Siegel D A, McClain C R, Sarmiento J L, Feldman G C, Milligan A J, Falkowski P G, Letelier R M and Boss E S 2006 Climate-driven trends in contemporary ocean productivity *Nature* **444** 752–5

[18] Raitsos D E Pradhan Y, Lavender S J, Hoteit I, McQuatters-Gollop A, Reid P C and Richardson A J 2014 From silk to satellite: half a century of ocean colour anomalies in the Northeast Atlantic *Glob. Change Biol.* **20** 2117–23

[19] Henson S A Humphreys M P, Land P E, Shutler J D, Goddijn-Murphy L and Warren M 2018 Controls on open-ocean North Atlantic Δp CO_2 at seasonal and interannual timescales are different *Geophys. Res. Lett.* **45** 9067–76

[20] Richardson A, Walne A and John A 2006 Using continuous plankton recorder data *Prog. Oceanogr.* **68** 27–74

[21] Landschützer P Gruber N, Bakker D C E, Schuster U, Nakaoka S, Payne M R, Sasse T P and Zeng J 2013 A neural network-based estimate of the seasonal to inter-annual variability of the Atlantic Ocean carbon sink *Biogeosciences* **10** 7793–815

[22] Landschützer P, Gruber N and Bakker D C E 2016 Decadal variations and trends of the global ocean carbon sink *Glob. Biogeochem. Cycles* **30** 1396–1417

[23] Bakker D C E *et al* 2016 A multi-decade record of high-quality fCO_2 data in version 3 of the Surface Ocean CO_2 Atlas (SOCAT) *Earth Syst. Sci. Data* **8** 383–413

[24] Dlugokency E, Masarie K, Lang P and Tans P 2014 Marine boundary layer reference NOAA greenhouse gas reference from atmospheric carbon dioxide dry air mole fractions from the NOAA ESRL carbon cycle cooperative global air sampling network (available at: www.esrl.noaa.gov/gmd/ccgg/mbl/)

[25] Reinfelder J R 2011 Carbon concentrating mechanisms in eukaryotic marine phytoplankton *Annu. Rev. Mar. Sci.* **3** 291–315

[26] Henson S, Le Moigne F and Giering S 2019 Drivers of carbon export efficiency in the global ocean *Glob. Biogeochem. Cycles* **33** 891–903

[27] Kortzinger A 1999 Determination of carbon dioxide partial pressure (p(CO_2)) *Methods of Seawater Analysis* (New York: Wiley)

[28] Dickson A, Sabine C and Christian J 2007 Guide to best practices for ocean CO_2 measurements *PICES Special Publication 3* (available at: www.vliz.be/imisdocs/publications/136635.pdf)

[29] Kalnay E *et al* 1996 The NCEP/NCAR 40-year reanalysis project (arXiv:1011.1669v3)

[30] Leterme S C, Edwards M, Reid P C and John A W G 2005 Decadal basin-scale changes in diatoms, dinoflagellates and phytoplankton color across the North Atlantic *Limnol. Oceanogr.* **50** 1244–53

[31] Owens N J P Hosie G W, Batten S D, Edwards M, Johns D G and Beaugrand G 2013 All plankton sampling systems underestimate abundance: response to "Continuous plankton recorder underestimates zooplankton abundance" by J.W. Dippner and M. Krause *J. Mar. Syst.* **128** 240–2

[32] Edwards M and Richardson A A J 2004 Impact of climate change on marine pelagic phenology and trophic mismatch *Nature* **430** 881–4

[33] Alvarez-Fernandez S, Lindeboom H and Meesters E 2012 Temporal changes in plankton of the North Sea: community shifts and environmental drivers *Mar. Ecol. Prog. Ser.* **462** 21–38

[34] Helaouët P, Beaugrand G and Edwards M 2013 Understanding long-term changes in species abundance using a niche-based approach *PLoS One* **8** e79186

[35] Sathyendranath S *et al* 2019 An ocean-colour time series for use in climate studies: the experience of the ocean-colour climate change initiative (OC-CCI) *Sensors* **19** 4285

[36] Woodruff S D 1987 A comprehensive ocean-atmos data set *Bull. Am. Meteorol. Soc.* **68** 1239–50

[37] Zuo H, Alonso-Balmaseda M, Mogensen K and Tietsche S 2018 OCEAN5: the ECMWF ocean reanalysis system and its real-time analysis component (available at: www.ecmwf.int/node/18519)

[38] Santer B D Wigley T M L, Boyle J S, Gaffen D J, Hnilo J J, Nychka D, Parker D E and Taylor K E 2000 Statistical significance of trends and trend differences in layer-average atmospheric temperature time series *J. Geophys. Res.* **105** 7337–56

[39] Pyper B J and Peterman R M 1998 Comparison of methods to account for autocorrelation in correlation analyses of fish data *Can. J. Fisheries Aquatic Sci.* **55** 2127–40

[40] Lovenduski N S, Gruber N and Doney S C 2008 Toward a mechanistic understanding of the decadal trends in the Southern Ocean carbon sink *Glob. Biogeochem. Cycles* **22** GB3016

[41] Glover D, Jenkins W and Doney S 2005 *Modeling Methods for Marine Science* (Cambridge: Cambridge University Press)

[42] Schmidtko S, Johnson G C and Lyman J M 2013 MIMOC: a global monthly isopycnal upper-ocean climatology with mixed layers *J. Geophys. Res.* **118** 1658–72

[43] Schuster U *et al* 2013 An assessment of the Atlantic and Arctic sea-air CO_2 fluxes, 1990-2009 *Biogeosciences* **9** 10669–724

[44] Takahashi T 2009 Climatological mean and decadal change in surface ocean pCO_2 and net sea-air CO_2 flux over the global oceans *Deep Sea Res.* II **56** 554–77

[45] Lovenduski N S, Long M C and Lindsay K 2015 Natural variability in the surface ocean carbonate ion concentration *Biogeosci. Discuss.* **12** 13123–57

[46] Lazier J, Hendry R, Clarke A, Yashayaev I and Rhines P 2002 Convection and restratification in the Labrador Sea, 1990–2000 *Deep-Sea Res.* I **49** 1819–35

[47] Stendardo I and Gruber N 2012 Oxygen trends over five decades in the North Atlantic *J. Geophys. Res.* **117** 1–18

[48] Doney S C 2006 Plankton in a warmer world *Nature* **444** 6–7

[49] Riebesell U, Körtzinger A and Oschlies A 2009 Sensitivities of marine carbon fluxes to ocean change *Proc. Natl Acad. Sci. USA* **106** 20602–9

[50] Bopp L *et al* 2013 Multiple stressors of ocean ecosystems in the 21st century: projections with CMIP5 models *Biogeosciences* **10** 6225–45

[51] Krumhardt K M, Lovenduski N S, Long M C and Lindsay K 2017 Avoidable impacts of ocean warming on marine primary production: insights from the CESM ensembles *Glob. Biogeochem. Cycles* **31** 114–33

[52] Gruber N 2009 Carbon cycle: fickle trends in the ocean *Nature* **458** 155–6

[53] Harris V, Edwards M and Olhede S C 2013 Multidecadal Atlantic climate variability and its impact on marine pelagic communities *J. Mar. Syst.* **113** 1–15

[54] Edwards M, Beaugrand G, Kléparski L, Hélaouët P and Reid P C 2022 Climate variability and multi-decadal diatom abundance in the Northeast Atlantic *Commun. Earth Environ.* **3** 162

[55] Osman M B Das S B, Trusel L D, Evans M J, Fischer H, Grieman M M, Kipfstuhl S, McConnell J R and Saltzman E S 2019 Industrial-era decline in subarctic Atlantic productivity *Nature* **569** 551–5

[56] Laufkötter C *et al* 2015 Drivers and uncertainties of future global marine primary production in marine ecosystem models *Biogeosci. Discuss.* **12** 3731–824